



JGR Space Physics

RESEARCH ARTICLE

10.1029/2021JA029981

Key Points:

- Density holes (DHs) are very common in the foreshock region and the average occurrence rate is ~5.4 events/day
- The occurrence rate of DHs is higher for faster solar wind, larger magnetic shear angle, and lower magnetic field strength
- Two thirds of DHs are different from other types of foreshock transients with low density and magnetic field strength cores

Supporting Information:

Supporting Information may be found in the online version of this article.

Correspondence to:

H. Zhang, hzhang14@alaska.edu

Citation:

Lu, X., Zhang, H., Liu, T., Vu, A., Pollock, C., & Wang, B. (2022). Statistical study of foreshock density holes. *Journal of Geophysical Research: Space Physics*, *127*, e2021JA029981. https://doi.org/10.1029/2021JA029981

Received 17 SEP 2021 Accepted 10 MAR 2022

Statistical Study of Foreshock Density Holes

Xi Lu¹ , Hui Zhang¹ , Terry Liu^{1,2} , Andrew Vu¹ , Craig Pollock³ , and Boyi Wang¹

¹Geophysical Institute, University of Alaska Fairbanks, Fairbanks, AK, USA, ²Cooperative Programs for the Advancement of Earth System Science, University Corporation for Atmospheric Research, Boulder, CO, USA, ³Denali Scientific, Fairbanks, AK, USA

Abstract Density holes (DHs), characterized by the correlating depletion of plasma density and magnetic field strength, are one of the transient structures frequently observed upstream of Earth's bow shock. The low dynamic pressure of DHs may disturb the bow shock and magnetopause, and have potential geoeffects. In this paper, we perform a statistical study of 411 density hole events, identified by the Magnetospheric Multiscale Mission. The average occurrence rate of DHs is \sim 5.4 events/day. All DHs are associated with foreshock ions. DHs tend to occur on the dawn side than on the dusk side. The occurrence rate is higher for faster solar wind, larger magnetic shear angle across DHs, and lower magnetic field strength. The spatial scale of DHs is several R_E . Within DHs, electron heating and density depletion are correlated. Most DHs do not have significant flow deflections. Most DHs with discontinuities have the convection electric field pointing toward the discontinuity on at least one side. About two thirds of the 411 events show different characteristics compared to other types of foreshock transients that also have correlated density and field strength depletion.

1. Introduction

Earth's bow shock is formed by the interaction of the solar wind with the Earth's magnetic dipole field. Upstream from the Earth's bow shock, the region filled with thermal back-streaming ions (Eastwood et al., 2005) is called the ion foreshock. These back-streaming ions can interact with the solar wind beam and generate ultralow frequency (ULF) waves (Wilson III, 2016). Inside the foreshock, there are various transient structures (Zhang et al., 2022), such as hot flow anomalies (HFAs) (Lin, 1997; Schwartz et al., 1985; Thomsen et al., 1988; Zhang et al., 2010), spontaneous hot flow anomalies (SHFAs) (Omidi et al., 2013; Zhang et al., 2013), foreshock bubbles (FBs) (Liu et al., 2015; Omidi et al., 2010, 2020; Turner et al., 2013, 2020), foreshock cavities (Billingham et al., 2008; Sibeck et al., 2002, 2021), and foreshock cavitons (Blanco-Cano et al., 2009, 2011; Kajdič et al., 2013; Wang et al., 2020). These foreshock transients have a common characteristic in that they have core regions with depletion in both density and field strength. HFAs, SHFAs, and FBs also have significant plasma heating and deflection within core regions. Additionally, the foreshock side of foreshock compressional boundaries (FCBs) sometimes also has low density and low field strength core regions (Rojas-Castillo et al., 2013). The spatial scales of their core regions range from \sim 1 to $10~R_E$.

Density holes (DHs) (Parks et al., 2006; Wilber et al., 2008) are transient structures observed in the solar wind and are also characterized by density dips accompanied by magnetic field dips with time durations of \sim 18 s and spatial scales of several thousand km (Parks et al., 2006).

DHs have relatively small magnetic shear angles across them and are not always associated with significant flow deflection and heating within them (Parks et al., 2006; Wilber et al., 2008). Almost all the DHs are embedded in the back-streaming foreshock ions. One possible formation mechanism is that the cold solar wind ions are squeezed out by the foreshock ions, making the core region low-density and heated (Wilber et al., 2008). The characteristics of DHs are mostly overlapped with many types of foreshock transients that are well identified in past studies. It thus becomes necessary to revisit DHs and determine whether DHs are a unique type of foreshock transient. Additionally, DHs, due to their low dynamic pressure, can potentially disturb the bow shock and magnetopause. It is therefore also important to examine their occurrence rate and favorable formation conditions. Using data from the Magnetospheric Multiscale (MMS) Mission, we perform a statistical analysis of 411 DHs observed in the solar wind from 2017 to 2019. In Section 2, we introduce the instruments we use and describe our event selection criteria. In Section 3, we show a typical DH example. Then the statistical results of DHs' characteristics and favorable interplanetary magnetic field (IMF)/solar wind conditions are presented in Section 4. We discuss and summarize our results in Sections 5 and 6.

© 2022. American Geophysical Union. All Rights Reserved.

LU ET AL. 1 of 11



2. Data and Methods

MMS is a constellation mission of four spacecraft launched in 2015. We use the electron density, ion velocity, ion and electron temperatures, the energy spectra from the Fast Plasma Investigation (FPI) (Pollock et al., 2016), and the magnetic fields from the Fluxgate Magnetometers (FGM) (Torbert et al., 2016a) in fast survey mode. We use the Advanced Composition Explorer (ACE) (Stone et al., 1998), and OMNI database (King & Papitashvili, 2005) for the solar wind velocity, density, and magnetic field for normalization.

We establish an event list of 411 DHs with Magnetospheric Multiscale 1 (MMS1) in the solar wind from October 2017 to April 2018 and October 2018 to May 2019 (~15 months). We use the solar wind time intervals from Vu et al. (2022) through machine learning and note that the presence of the foreshock region is not a requirement to investigate whether DHs could be solar wind structures.

Then we use the criteria listed below to identify DHs.

- 1. The density depletion in the hole region should reach 20% compared to the ambient solar wind value. The density depletion is calculated by $(n_{ave} n_{min})/n_{ave}$, where n_{ave} is the 5-min averaged density, and n_{min} is the density minimum inside the hole.
- 2. The variation of the magnetic field correlates with the density depletion in the hole region (Parks et al., 2006). The correlation coefficient of the electron density and the magnetic field strength should be larger than 0.5.
- 3. To distinguish DHs from HFAs, SHFAs, FBs, and foreshock cavities to some extent, the duration of DHs needs to be shorter than 1 min.
- 4. To exclude fast mode wave trains, a variable has been used, $\chi(t) = [n(t) \langle n \rangle] \cdot [B(t) \langle B \rangle]$, where $\langle n \rangle$ and $\langle B \rangle$ are the average values of the 5-min interval (Kajdič et al., 2013). To obtain isolated events, the value of χ for the events must be at least 3 standard deviations larger than the average of χ , that is, $f(\chi) = (\chi(t) \langle \chi \rangle)/std(\chi) > 3$, where $\langle \chi \rangle$ is the 5-min averaged χ and $std(\chi)$ is the standard deviation of χ .
- 5. If events are embedded in large ULF fluctuations (Kajdič et al., 2013), the value of χ for the events must be at least 5 standard deviations larger than the average of χ , that is, $f(\chi) = (\chi(t) \langle \chi \rangle)/std(\chi) > 5$.

For each event, we determine the duration of DHs by choosing when the electron densities raised back from the density minimum to no more than 1/e of the 5-min average. The ambient time intervals for the background quantities are determined manually to ensure that we exclude any discontinuities, bow shock crossing, and other foreshock transients nearby. We calculate solar wind parameters, IMF parameters, and foreshock ion parameters in the core region and in the ambient time intervals. We use the Merka et al. (2005) bow shock model to calculate the normal at the local bow shock that is closest to the spacecraft. We calculate the moments of foreshock ions from ion velocity distributions after removing the solar wind ion beam (Liu et al., 2017). When comparing the foreshock ion properties in DHs with the background, we select the side (upstream or downstream) where the foreshock ion density is closer to that in the DH (suggesting that such a side is more likely the foreshock ion source). We also calculate the moments of pristine solar wind ions by using MMS FPI distributions to compare flow deflection, and we use OMNI 1-min resolution data to obtain the occurrence conditions.

3. Case Study

Figure 1 shows an example DH observed on 7 February 2018. In this case, the electron density and magnetic field strength are correlated in the core region with a duration of 27 s. The density depletion is 33.7%. The ion bulk velocity remains the same during the wholetime interval. Electron temperatures do not show an obvious increase compared to the ambient regions. From the ion energy spectra (Figure 1h), we can see that the DH is embedded in back-streaming foreshock ions and the foreshock ion density increases (Figure 1c). The ion temperature is dominated by the presence of foreshock ions, and thus the ion temperature (Figure 1g) correlates with the foreshock ion density (Figure 1c). The maximum $f(\chi)$ is larger than three, suggesting that the variation is significant enough compared to the background.

Since the ion bulk velocity is barely deflected and the electrons are not heated but rather cooled (Figure 1f), this event cannot be categorized as HFAs (Zhang et al., 2010), SHFAs (Zhang et al., 2013), or FBs (Liu et al., 2015). Because this DH is embedded in the foreshock ions on the upstream side, this is not a foreshock cavity (Billingham

LU ET AL. 2 of 11

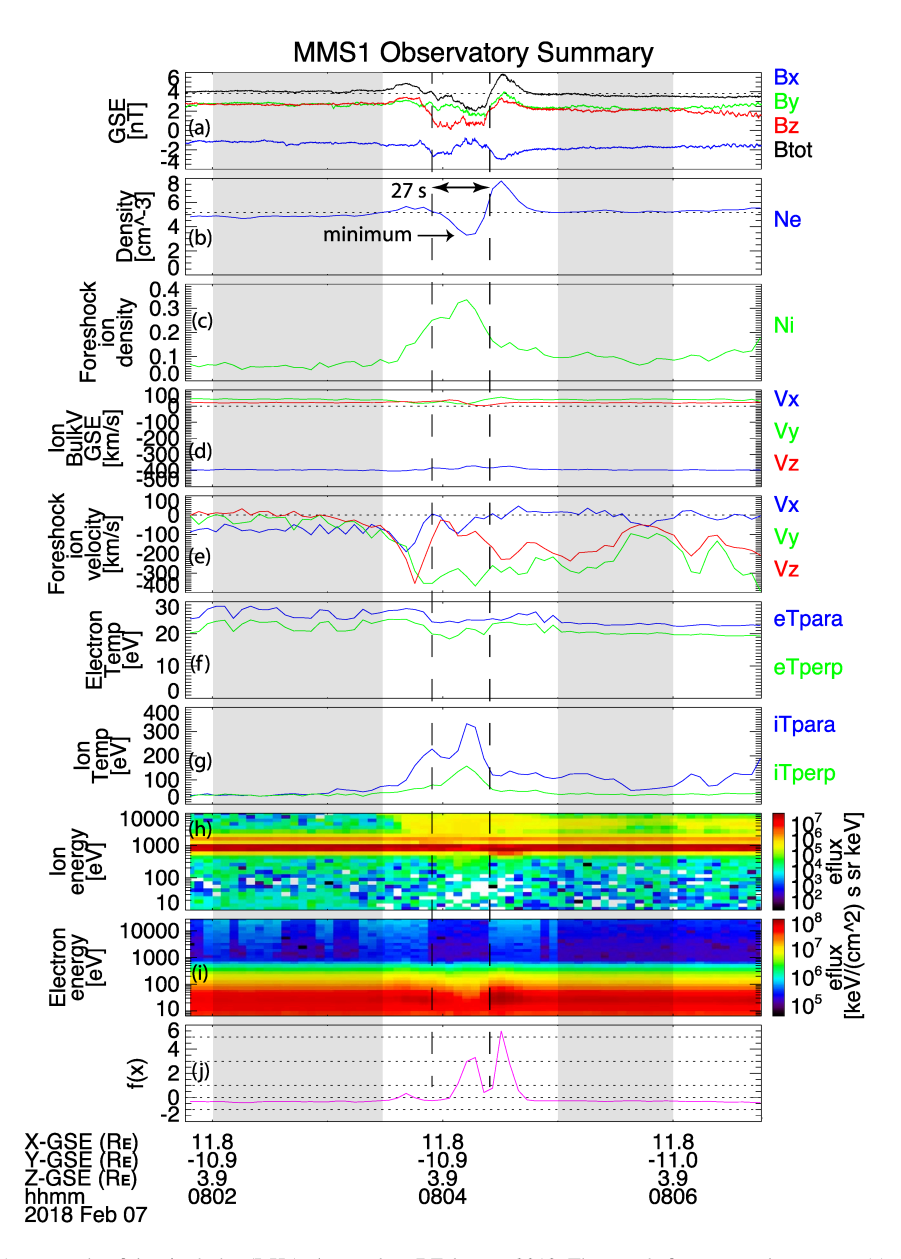


Figure 1. An example of density holes (DHs) observed on 7 February 2018. The panels from top to bottom are (a) magnetic field components and strength in geocentric solar ecliptic (GSE) coordinates, (b) the electron density, (c) the foreshock ion density, (d) the ion bulk velocity, (e) the foreshock ion velocity, (f) parallel and perpendicular temperatures of the electrons, (g) parallel and perpendicular temperatures of the ions (including solar wind and foreshock ions), (h) ion energy spectra, (i) electron energy spectra, and (j) function χ . The horizontal dashed lines in panels (a, b) are the averaged values of magnetic field strength and the electron density during the whole interval, respectively. The five dashed lines in (j) represent the function χ equals 5, 3, 0, and plus/minus one standard deviation of the function, respectively.

et al., 2008). This event should not be a foreshock caviton (Kajdič et al., 2013) because ULF waves were not present. This event is not a typical FCB (Rojas-Castillo et al., 2013) either, because the compression is stronger on the foreshock side. Therefore, this event cannot be categorized as any of these known types of foreshock transients and should be a unique type. After the statistical study, we will discuss what percentage of our events belong to a unique type.

LU ET AL. 3 of 11

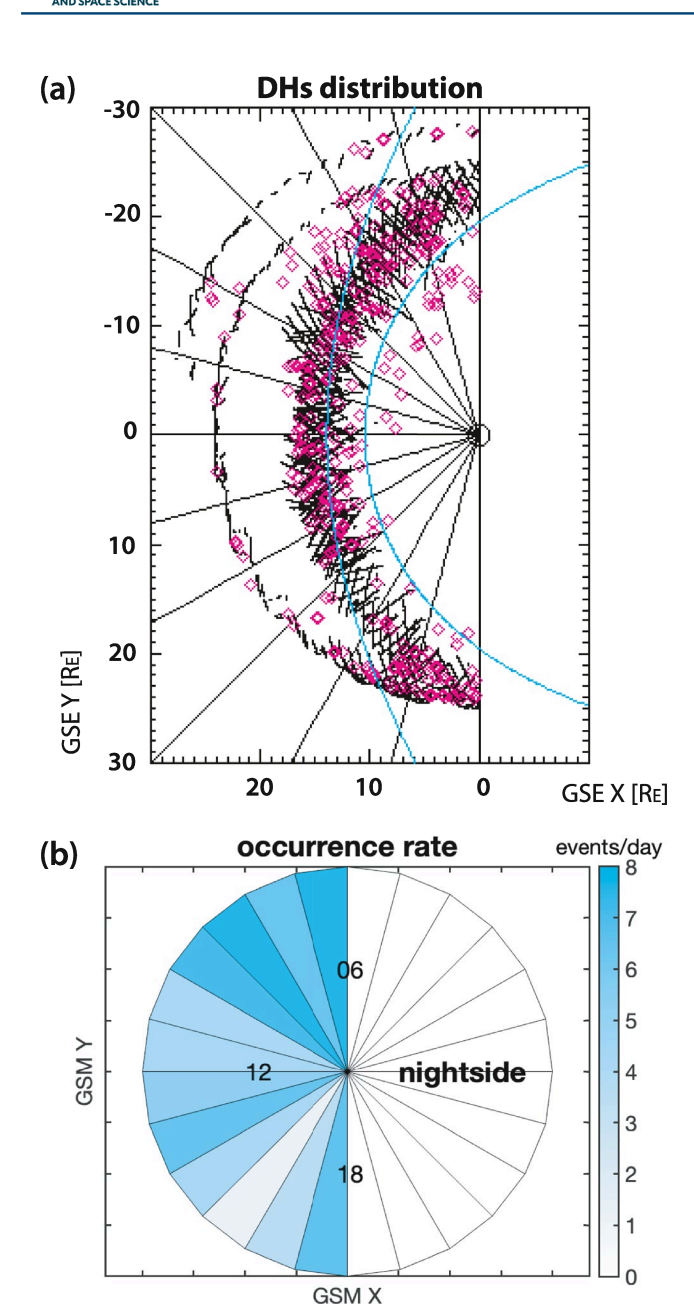


Figure 2. Panel (a) is the Magnetospheric Multiscale 1 (MMS1) orbits (black curves) in the solar wind during the 15-month interval with density holes (DHs) locations (pink diamonds) and the averaged bow shock and magnetopause (blue curves). Panel (b) shows the occurrence rate of DHs as a function of MLT. The numbers shown within the circle are MLTs.

4. Statistical Study

The total time that MMS1 spent in the solar wind between October 2017–April 2018 and October 2018–May 2019 is ~76 days, and MMS1 observed 411 DHs. The average occurrence rate is therefore 5.4 events/day, which is larger than the occurrence rate of HFAs (Schwartz et al., 2000) and foreshock cavities (Billingham et al., 2008; Sibeck et al., 2001).

4.1. Properties of DHs

Figure 2a gives an overview of DHs' positions, average bow shock and magnetopause positions, and MMS1 orbits. Figure 2b shows the occurrence rate of DHs in different magnetic local time (MLT). The occurrence rates on the dawn side (6–10 MLT) and on the dusk side (14–18 MLT) are \sim 44.8% and \sim 23.9%, respectively. Such a dawn-dusk asymmetry is likely due to the Parker spiral IMF configuration.

Figure 3 shows the characteristics of DHs. Most events are between 13.5 and 40.5 s in duration and the mean value of all events is ~ 30.3 s (Figure 3a). The mean electron density depletion (Figure 3b) is $\sim 41.9\%$ and the number of events decreases with increasing electron density depletion. Since the magnetic field strength needs to be correlated with the density, the mean depletion of magnetic field strength (Figure 3c) is $\sim 35.3\%$, similar to the mean density depletion.

Figures 3d and 3g show the portion distributions of the ratio of ion speed (with and without foreshock ions, respectively) along the local bow shock normal inside DHs and the background. Without foreshock ions, the speed depletion becomes smaller. Figures 3e and 3h show the portion distributions of the maximum angles between the ion velocity (with and without foreshock ions, respectively) in DHs and in the background. Both show very small deviation angles, mainly from 1.5° to 6.0° , indicating that most DHs do not have significant flow deflections (A few events with deviation angles above 18° are not shown). By comparing these two plots, the flow deviation angles are also affected by the presence of foreshock ions.

For each event, when the magnetic shear angle across it is less than 15°, the event is defined as no discontinuity. For an event without discontinuities, we assume that the event convects with the solar wind (Figure 3f) and calculate its spatial scale along geocentric solar ecliptic (GSE)-X direction using $V_{bulk}|_x \cdot \Delta t$, where the $V_{bulk}|_x$ is the GSE-X component of the bulk flow velocity averaged inside the DH and Δt is the duration. For an event with discontinuities, we assume the discontinuity is a tangential discontinuity (Figure 3i) and the discontinuity's propagation determines how the structure crosses the spacecraft. Therefore, the scale length is measured along its propagation direction along the bow shock surface, that is, $V_{tr} \cdot \Delta t$, where the transit velocity is $V_{tr} = V_{sw} \cdot n_{cs}/\sin^2\theta_{cs:bs}(n_{cs} - cos\theta_{cs:bs}n_{cs})$, and the discontinuity (current sheet) normal is $n_{cs} = B_u \times B_d/B_u \times B_d$, and $\theta_{cs:bs}$ is the angle between the

discontinuity normal and the bow shock normal (Schwartz et al., 2000). The mean spatial scales of DHs are \sim 1.89 R_E without discontinuities (168 out of 411) and \sim 1.32 R_E with discontinuities (243 out of 411). These scales are comparable to HFAs (Facskó et al., 2009). For each event, we also use the timing analysis (Paschmann & Schwartz, 2000) to calculate the normal speed of downstream and upstream boundaries of DHs and use their average to calculate the size. The results based on timing for events with and without discontinuities are qualitatively comparable to each other (Figure S2 in Supporting Information S1). However, because the time resolution of magnetic field data in fast mode (0.0625 s) is very close to the time delay between two spacecraft, the results have large uncertainties.

LU ET AL. 4 of 11

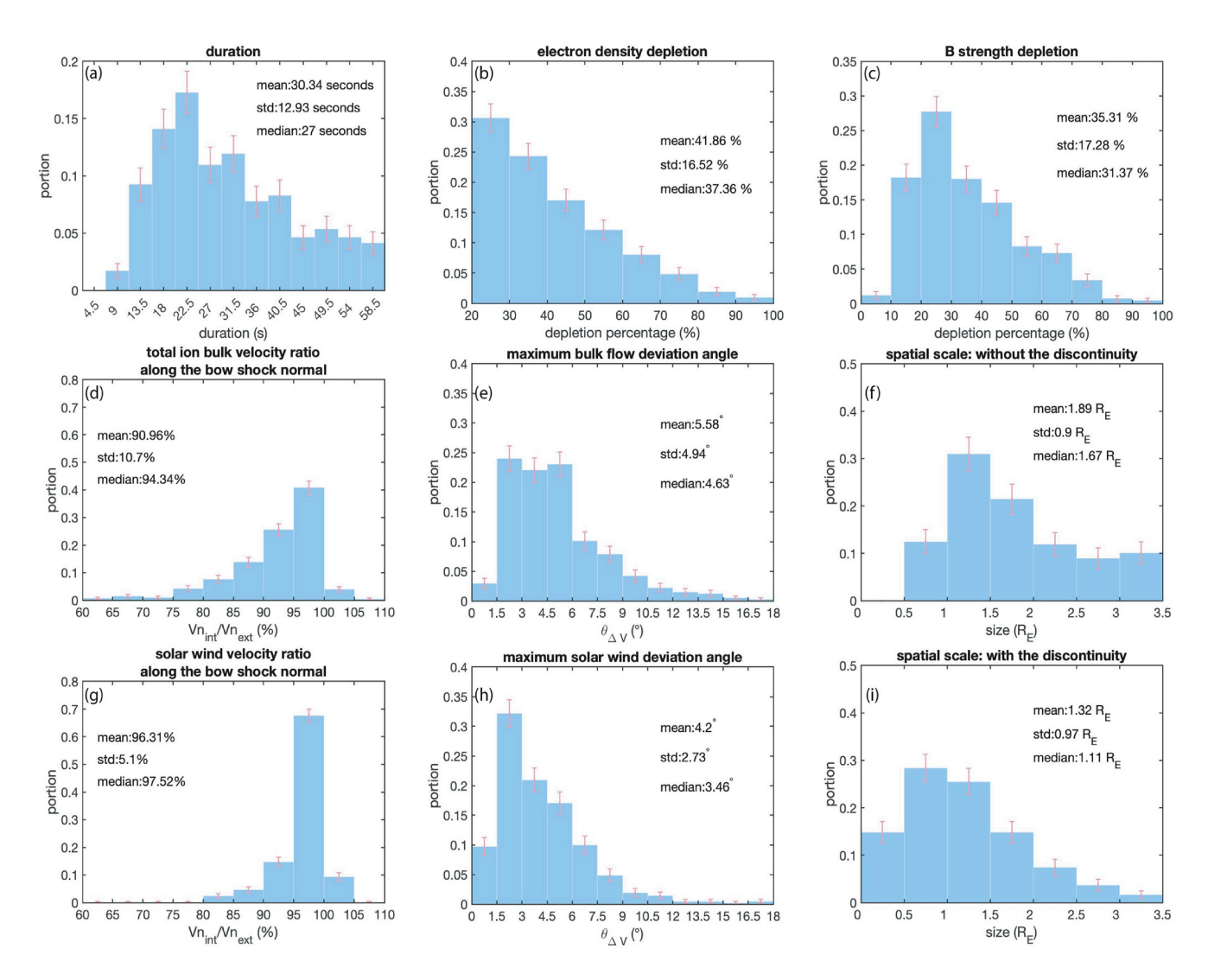


Figure 3. The portion distributions of (a) duration, (b) electron density depletion, (c) magnetic field strength depletion, (d) total ion bulk velocity ratio along the bow shock normal, (e) maximum bulk flow deviation angle, (f) spatial scale of density holes (DHs) without discontinuities, (g) solar wind velocity (without foreshock ions) ratio along the bow shock normal, (h) maximum solar wind deviation angle and (i) spatial scale of DHs with discontinuities. The text provides the mean value, standard deviation value, and median value for each distribution.

Figures 4a and 4b show that the ratios of perpendicular and parallel electron temperatures inside the DHs to that of the background are correlated with the density depletion, respectively. The correlation between the electron heating and density depletion for events with density depletion greater than 1/3 (blue dots and red dashed line) is better than that for all events (black dashed line).

Figures 4c and 4d are the ratio of perpendicular temperature anisotropy inside DHs to that in the ambient region for electrons and foreshock ions, respectively. For small density depletion events, the electrons show enhanced parallel anisotropy compared to the background. The electron perpendicular anisotropy is more likely to enhance for some larger density depletion events. For foreshock ion temperature, most events show enhanced perpendicular anisotropy, without a clear tendency to the density depletion.

Figures 5a–5f show the comparison of the foreshock ion density and energy inside DHs and the background. The events without foreshock ions on both sides are excluded. The foreshock ion density (Figure 5a) inside the DH is close to or higher than that in the background, consistent with case studies by Liu et al. (2017, 2020). The perpendicular temperature (Figure 5c) inside DHs is overall higher than that in the background, while the parallel temperature (Figure 5d) shows the opposite (consistent with Figure 4d). And the average temperature (Figure 5e) in DHs is very similar to that in the background. As the bulk kinetic energy (Figure 5b) does not change much as

LU ET AL. 5 of 11

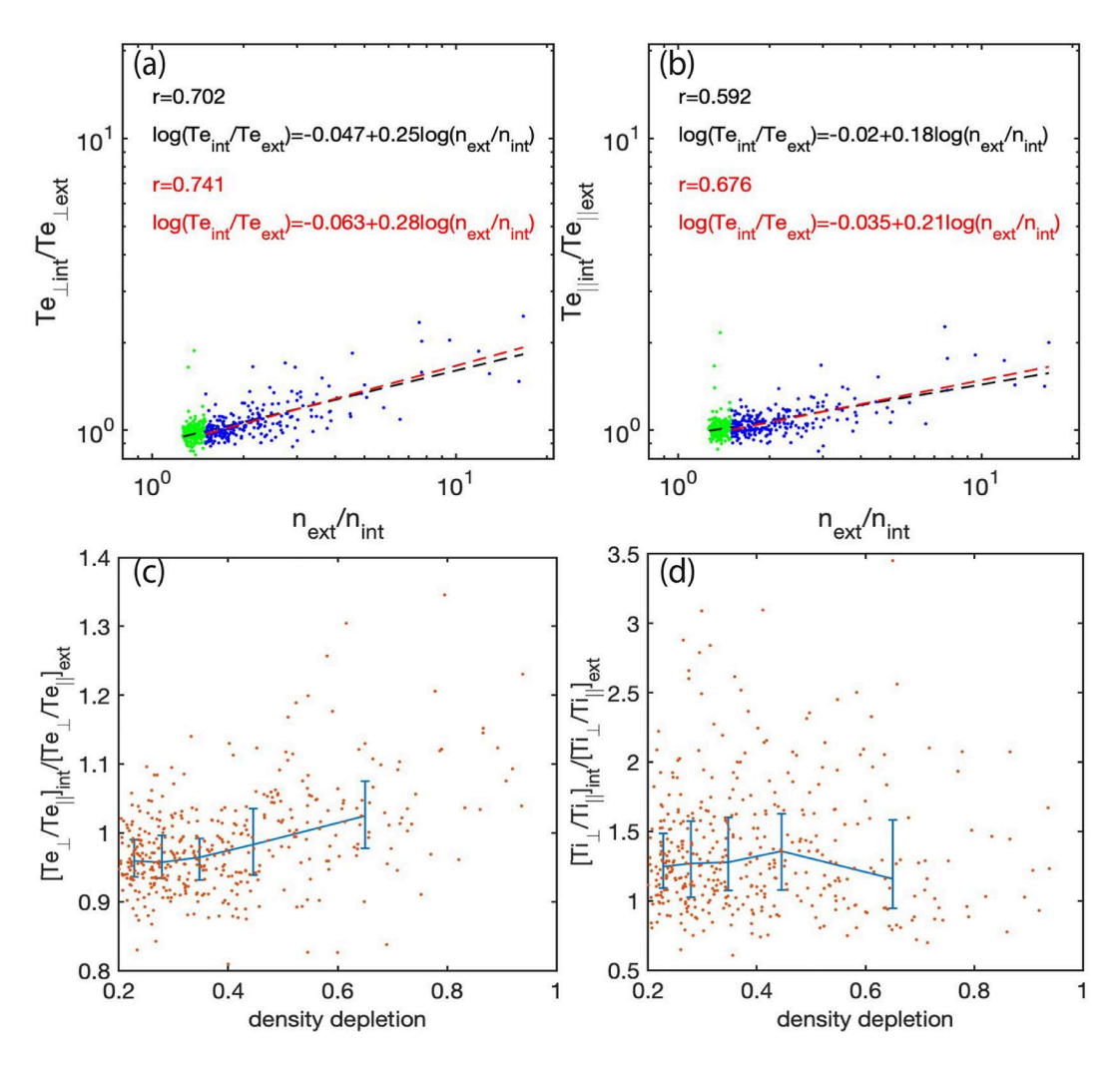


Figure 4. Scatter plots of (a) perpendicular electron temperature ratio versus density ratio, (b) parallel electron temperature ratio versus density ratio. (c) The ratio of perpendicular electron temperature and parallel electron temperature within density holes (DHs) over that in the ambient versus density depletion, and (d) the ratio of perpendicular foreshock ion temperature and parallel foreshock ion temperature within DHs over that in the ambient versus density depletion. The subscript *ext* and *int* mean the average density values of the ambient and the DH, respectively. The blue (green) dots in (a) and (b) are the events with their density depletions larger (smaller) than 1/3. The black dashed lines in (a) and (b) are the linear fit for all events while the red dashed lines are only for the blue dot events.

well, DHs have almost the same total foreshock ion energy (Figure 6f, the sum of bulk kinetic energy and average temperature) as the background.

4.2. Solar Wind Conditions

Next, we examine the favorable solar wind/IMF conditions of DHs. In Figure 6a, the top panel shows the portion distribution of DHs. All events except one have magnetic shear angles less than 140°. The middle panel provides the shear angles across solar wind discontinuities during the same 15 months of the event list by using the partial variance of increment (PVI) method at ACE (Liu et al., 2021; Wang et al., 2013; Zhao et al., 2017). The bottom panel shows the occurrence rate based on the upper two panels, which is higher for larger magnetic shear angle.

Figure 6b is for the IMF cone angle (angle between GSE-X and IMF) downstream the DHs in the same format as in Figure 5a. Because many of our events are in the flank region (Figure 1), the relationship between the occurrence rate and cone angles is not clear.

LU ET AL. 6 of 11

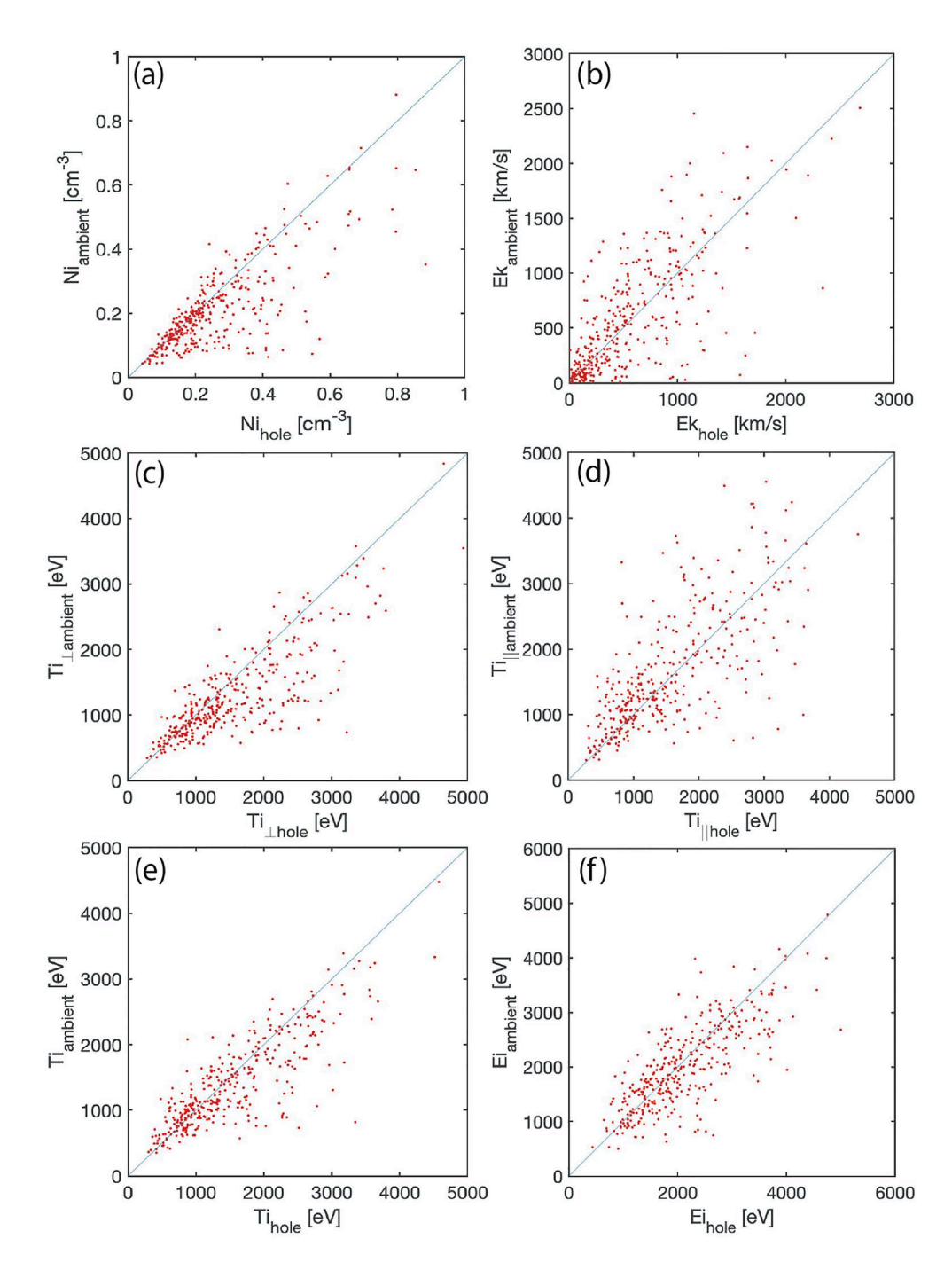


Figure 5. (a–f) are the averaged density, bulk kinetic energy, perpendicular temperature, parallel temperature, average temperature and total energy of foreshock ions inside the density holes regions compared to the background.

Figures 6c–6e show the occurrence rates as a function of the ambient solar wind electron density, the ambient solar wind velocity, and the ambient magnetic field strength, respectively. They show that the occurrence rate is higher for lower solar wind density, faster solar wind speed, and weaker magnetic field strength. The dependence of the occurrence rate on the density is due to the fact that faster solar wind has lower density (Figure S1 in Supporting Information S1).

Figure 6f shows the occurrence rate as a function of the angle (θ_{Bn}) between the bow shock normal and magnetic field. As shown in the top panel, 75.8% of DHs are embedded in the quasi-parallel region $(\theta_{Bn} < 45^{\circ})$ and over

LU ET AL. 7 of 11



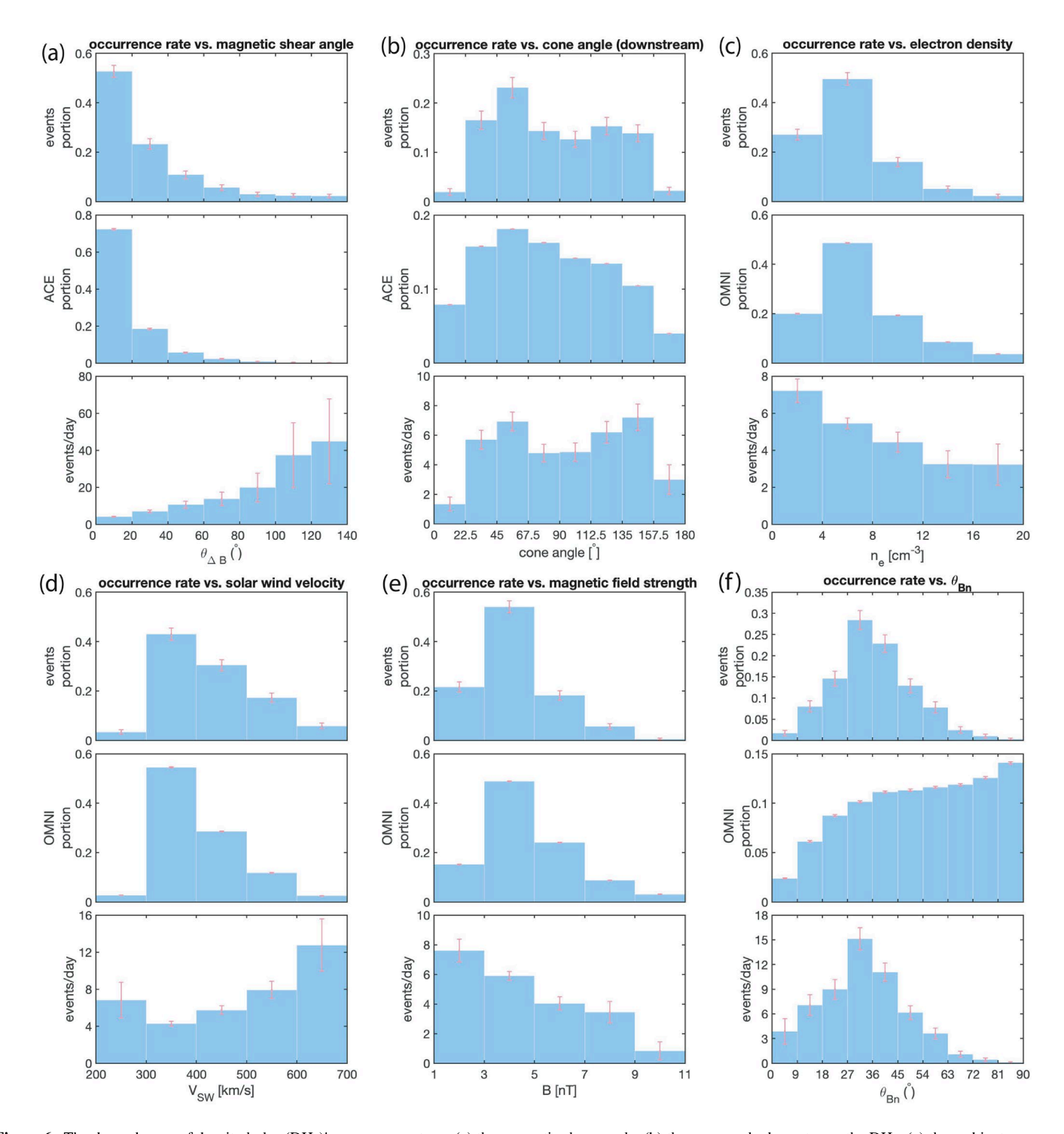


Figure 6. The dependences of density holes (DHs)' occurrence rate on (a) the magnetic shear angle, (b) the cone angle downstream the DHs, (c) the ambient electron density, (d) the ambient solar wind velocity, (e) the ambient magnetic field strength, and (f) θ_{Bn} . The data in the (f) middle panel use the OMNI data with Magnetospheric Multiscale (MMS) location.

95% of events have θ_{Bn} less than 60°. For the background (middle panel), we combine the OMNI data with MMS1's locations to calculate θ_{Bn} . This tendency for the background may be due to the MMS1's locations during that period. The occurrence rate (bottom panel) is higher in the quasi-parallel region and its maximum is at 27–36°.

LU ET AL. 8 of 11

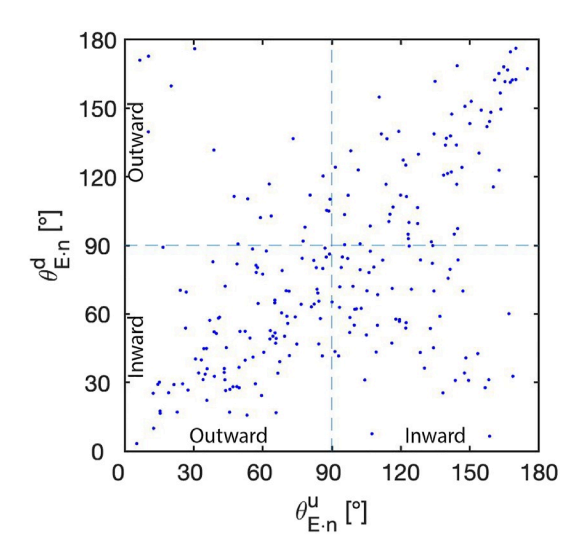


Figure 7. The scatter plot of angles between discontinuity normal and convection electric field. The superscript u and d represent the upstream and downstream of density holes. Since we define that n_{cs} is positive pointing sunward, angles between 0° and 90° (90°–180°) for upstream means pointing outward (inward) and for downstream it is the reverse.

For the DHs with a discontinuity (shear angles larger than 15°; 243 out of 411 DHs), the angles between the discontinuity normal and the convection electric field are calculated on two sides (Figure 7). 223 (out of 243) events have electric fields on at least one side pointing toward discontinuities. Among these 223 events, 60 events have electric fields on both sides pointing toward the discontinuity.

5. Discussion

When we selected DHs, we did not require the foreshock region in the background. But the DHs we identified from 2017 to 2019 are mostly embedded in the foreshock region or have foreshock ions within them (like foreshock cavities). Only several events could be the solar wind structures.

In Figure 6f, the majority of DHs appear in the quasi-parallel foreshock region. However, the very small θ_{Bn} is not the most favorable condition for the formation of DHs. The reason needs to be further examined (e.g., the too fluctuated magnetic field or very diffuse foreshock ions may not favor the formation, and the propagation of DHs could differ the observed θ_{Bn} from the one at the formation position).

In the statistical study by Wilber et al. (2008), the ion temperature ratio (internal/external) is correlated well with ion density depletion (external/internal), because of the increase in foreshock ion density ratio to the solar wind ion

density. Here we find the same tendency for the perpendicular and parallel electron temperature ratios (internal/external) and density ratio (external/internal) (Figures 4a and 4b). The perpendicular anisotropy is also enhanced when the density and field strength depletion is strong (Figure 4c). These results suggest that the electron heating is nonadiabatic, and the mechanisms need further investigation in the future.

Next, we categorize our events based on the characteristics of other types of foreshock transients (Table S1 in Supporting Information S1). An event is categorized as an HFA when it shows a 20% bulk flow speed decrease along the bow shock normal, a 20% ion temperature increase, and a magnetic shear angle larger than 15°. An event categorized as an SHFA shares the same characteristics, except that its magnetic shear angle needs to be less than 15°. The criteria for being an FB consist of a more than 20% bulk flow speed decrease in the bow shock normal direction, an increase in the ion temperature, and significant enhancements of density and magnetic field strength (shock) on the upstream side of the core. The events embedded in waves with ion temperature increase and bulk flow speed decrease of less than 20% are foreshock cavitons. Ion energy spectra are used to categorize FCBs and foreshock cavities. FCBs have enhancements of density and magnetic field strength on the boundary that separates the pristine solar wind and the foreshock, whereas foreshock cavities have no foreshock ions on either side.

We find that 15.1% (62 out of 411) of the events show the cavities' characteristics. 8.3% (34 out of 411) are cavitons, where 6 (out of 34) of them are typical cavitons without the ion temperature increase and the rest are associated with heating. 5.8% (24 out of 411) are HFAs and 2.7% (11 out of 411) are SHFAs. Only 1.5% (6 out of 411) belong to FCBs and 0.5% (2 out of 411) are FBs. About two thirds of our events cannot be categorized as any of these types of foreshock transients. Therefore, our DHs include unique types of foreshock transients that require further studies to identify their nature.

6. Summary and Conclusions

From October 2017 to April 2018 and October 2018 to May 2019, 411 DH events were observed by MMS1 in the solar wind. Most DH events are in the foreshock and/or associated with foreshock ions inside them. They have an average occurrence rate of 5.4 events/day. They occur at 6–18 MLTs (the cutoff at 6 MLT and 18 MLT is due to the separation of the dayside and nightside) upstream from the bow shock and the occurrence is higher on the dawn side than that on the dusk side. Most DHs do not have significant flow deflection. The average duration of DHs is 30.3 s and their spatial scales are 0.5–2 $R_{\rm E}$. The electron temperature ratio (internal/external) is correlated

LU ET AL. 9 of 11



well with electron density depletion. For most DH events, the foreshock ions show enhanced perpendicular anisotropy without clear energy change inside the DHs compared to the background. The occurrence rate of DHs is higher for larger magnetic shear angle, faster solar wind speed, and lower magnetic field strength. Most of them are in the quasi-parallel foreshock region, and the highest occurrence rate is at θ_{Bn} around 30°. For the events with discontinuities, most of them have an electric field pointing toward discontinuities on at least one side. About two thirds of the events cannot be categorized as other types of foreshock transients. Further case studies are needed to reveal the nature of these DHs.

Data Availability Statement

The MMS1 data can be obtained from https://lasp.colorado.edu/mms/sdc/public/. The ACE spacecraft data and the OMNI data are available at https://omniweb.gsfc.nasa.gov.

Acknowledgments

The work is supported by NASA award 80NSSC20K1513 and NSF AGS-13526669. T. Z. Liu is supported by the NASA Living With a Star Jack Eddy Postdoctoral Fellowship Program, administered by the Cooperative Programs for the Advancement of Earth System Science (CPAESS). T. Z. Liu is partially supported by NSF award AGS-1941012.

References

- Billingham, L., Schwartz, S. J., & Sibeck, D. G. (2008). The statistics of foreshock cavities: Results of a cluster survey. *Annals of Geophysics*, 26, 3653–3667. https://doi.org/10.5194/angeo-26-3653-2008
- Blanco-Cano, X., Kajdič, P., Omidi, N., & Russell, C. T. (2011). Foreshock cavitons for different interplanetary magnetic field geometries: Simulations and observations. *Journal of Geophysical Research*, 116, A09101. https://doi.org/10.1029/2010JA016413
- Blanco-Cano, X., Omidi, N., & Russell, C. T. (2009). Global hybrid simulations: Foreshock waves and cavitons under radial interplanetary magnetic field geometry. *Journal of Geophysical Research*, 114, A01216. https://doi.org/10.1029/2008JA013406
- Eastwood, J. P., Lucek, E. A., Mazelle, C., Meziane, K., Narita, Y., Pickett, J., & Treumann, R. A. (2005). The foreshock. Space Science Reviews, 118, 41–94. https://doi.org/10.1007/s11214-005-3824-3
- Facskó, G., Németh, Z., Erdős, G., Kis, A., & Dandouras, I. (2009). A global study of hot flow anomalies using Cluster multi-spacecraft measurements. *Annals of Geophysics*, 27, 2057–2076. https://doi.org/10.5194/angeo-27-2057-2009
- Kajdič, P., Blanco-Cano, X., Omidi, N., Meziane, K., Russell, C. T., Sauvaud, J.-A., & Lavraud, B. (2013). Statistical study of foreshock cavitons. Annales de Geophysique, 31, 2163–2178. https://doi.org/10.5194/angeo-31-2163-2013
- King, J. H., & Papitashvili, N. E. (2005). Solar wind spatial scales in and comparisons of hourly Wind and ACE plasma and magnetic field data. Journal of Geophysical Research, 110, A02104. https://doi.org/10.1029/2004JA010649
- Lin, Y. (1997). Generation of anomalous flows near the bow shock by its interaction with interplanetary discontinuities. *Journal of Geophysical Research*, 102(24), 24265–24281. https://doi.org/10.1029/97JA01989
- Liu, T. Z., An, X., Zhang, H., & Turner, D. (2020). Magnetospheric Multiscale (MMS) observations of foreshock transients at their very early stage. *The Astrophysical Journal*, 902. https://doi.org/10.3847/1538-4357/abb249
- Liu, T. Z., Angelopoulos, V., Hietala, H., & Wilson, L. B., III (2017). Statistical study of particle acceleration in the core of foreshock transients. Journal of Geophysical Research: Space Physics, 122, 7197–7208. https://doi.org/10.1002/2017JA024043
- Liu, T. Z., Zhang, H., Wang, C.-P., Angelopoulos, V., Vu, A., Wang, X., & Lin, Y. (2021). Statistical study of foreshock transients in the midtail foreshock. *Journal of Geophysical Research: Space Physics*, 126, e2021JA029156. https://doi.org/10.1029/2021JA029156
- Liu, Z., Turner, D. L., Angelopoulos, V., & Omidi, N. (2015). THEMIS observations of tangential discontinuity-driven foreshock bubbles. Geophysical Research Letters, 42, 7860–7866. https://doi.org/10.1002/2015g1065842
- Merka, J., Szabo, A., Slavin, J. A., & Peredo, M. (2005). Three-dimensional position and shape of the bow shock and their variation with upstream Mach numbers and interplanetary magnetic field orientation. *Journal of Geophysical Research*, 110, A04202. https://doi.org/10.1029/2004ja010944
- Omidi, N., Eastwood, J. P., & Sibeck, D. G. (2010). Foreshock bubbles and their global magnetospheric impacts. *Journal of Geophysical Research*, 115, A06204. https://doi.org/10.1029/2009JA014828
- Omidi, N., Lee, S. H., Sibeck, D. G., Turner, D. L., Liu, T. Z., & Angelopoulos, V. (2020). Formation and topology of foreshock bubbles. *Journal of Geophysical Research: Space Physics*, 125, e2020JA028058. https://doi.org/10.1029/2020JA028058
- Omidi, N., Zhang, H., Sibeck, D., & Turner, D. (2013). Spontaneous hot flow anomalies at quasi-parallel shocks: 2. Hybrid simulations. *Journal of Geophysical Research: Space Physics*, 118, 173–180. https://doi.org/10.1029/2012JA018099
- Parks, G., Lee, E., Mozer, F., Wilber, M., Lucek, E., Dandouras, I., et al. (2006). Larmor radius size density holes discovered in the solar wind
- upstream of Earth's bow shock. *Physics of Plasmas*, 13, 050701. https://doi.org/10.1063/1.2201056

 Paschmann, G., & Schwartz, S. J. (2000). ISSI book on analysis methods for multi-spacecraft data. *Cluster-II workshop multiscale/multipoint*
- plasma measurements (Vol. 449, p. 99). ESA Special Publication.

 Pollock, C., Moore, T., Jacques, A., Burch, J., Gliese, U., Saito, Y., et al. (2016). Fast plasma investigation for magnetospheric multiscale. Space Science Reviews. 199, 331–406. https://doi.org/10.1007/s11214-016-0245-4
- Rojas-Castillo, D., Blanco-Cano, X., Kajdič, P., & Omidi, N. (2013). Foreshock compressional boundaries observed by Cluster. *Journal of*
- Geophysical Research: Space Physics, 118, 698–715. https://doi.org/10.1029/2011JA017385
 Schwartz, S. J., Chaloner, C. P., Hall, D. S., Christiansen, P. J., Johnstone, A. D., Johnstone, A. D., et al. (1985). An active current sheet in the
- solar wind. *Nature*, 318, 269–271. https://doi.org/10.1038/318269a0
 Schwartz, S. J., Paschmann, G., Sckopke, N., Bauer, T. M., Dunlop, M., Fazakerley, A. N., & Thomsen, M. F. (2000). Conditions for the formation of hot flow anomalies at Earth's bow shock. *Journal of Geophysical Research*, 105, 12639–12650. https://doi.org/10.1029/1999JA000320
- Sibeck, D. G., Decker, R. B., Mitchell, D. G., Lazarus, A. J., Lepping, R. P., & Szabo, A. (2001). Solar wind preconditioning in the flank fore-shock: IMP 8 observations. *Journal of Geophysical Research*, 106, 21675–21688. https://doi.org/10.1029/2000ja000417
- Sibeck, D. G., Lee, S.-H., Omidi, N., & Angelopoulos, V. (2021). Foreshock cavities: Direct transmission through the bow shock. *Journal of Geophysical Research: Space Physics*, 126, e2021JA029201. https://doi.org/10.1029/2021JA029201
- Sibeck, D. G., Phan, T.-D., Lin, R., Lepping, R., & Szabo, A. (2002). Wind observations of foreshock cavities: A case study. *Journal of Geophysical Research*, 107, 1271. https://doi.org/10.1029/2001ja007539

LU ET AL. 10 of 11



- Stone, E., Frandsen, A., Mewaldt, R., Christian, E. R., Margolies, D., Ormes, J. F., & Snow, F. (1998). The advanced composition explorer. Space Science Reviews, 86, 1–22. https://doi.org/10.1023/A:1005082526237
- Thomsen, M. F., Gosling, J. T., Bame, S. J., Quest, K. B., Russell, C. T., & Fuselier, S. A. (1988). On the origin of hot diamagnetic cavities near the Earth's bow shock. *Journal of Geophysical Research*, 93, 11311–11325. https://doi.org/10.1029/JA093iA10p11311
- Torbert, R. B., Russell, C. T., Magnes, W., Ergun, R. E., Lindqvist, P.-A., LeContel, O., et al. (2016). The FIELDS instrument suite on MMS: Scientific objectives, measurements, and data products. *Space Science Reviews*, 199, 105–135. https://doi.org/10.1007/s11214-019-8
- Turner, D. L., Liu, T. Z., Wilson, L. B., III, Cohen, I. J., Gershman, D. G., Fennell, J. F., et al. (2020). Microscopic, multipoint characterization of foreshock bubbles with Magnetospheric Multiscale (MMS). *Journal of Geophysical Research: Space Physics*, 125, e2019JA027707. https://doi.org/10.1029/2019JA027707
- Turner, D. L., Omidi, N., Sibeck, D. G., & Angelopoulos, V. (2013). First observations of foreshock bubbles upstream of Earth's bow shock: Characteristics and comparisons to HFAs. *Journal of Geophysical Research: Space Physics*, 118, 1552–1570. https://doi.org/10.1002/jgra.50198
- Vu, A., Liu, T. Z., Zhang, H., & Pollock, C. (2022). Statistical study of foreshock bubbles, hot flow anomalies, and spontaneous hot flow anomalies and their substructures observed by MMS. *Journal of Geophysical Research: Space Physics*, 127, e2021JA030029. https://doi.org/10.1029/2021JA030029
- Wang, M., Yao, S., Shi, Q., Zhang, H., Tian, A., Degeling, A. W., et al. (2020). Propagation properties of foreshock cavitons: Cluster observations. Science China Technological Sciences, 63, 173–182. https://doi.org/10.1007/s11431-018-9450-3
- Wang, X., Tu, C., He, J., Marschand, E., & Wang, L. (2013). On intermittent turbulence heating of the solar wind: Differences between tangential and rotational discontinuities. *The Astrophysical Journal Letters*, 772, L14. https://doi.org/10.1088/2041-8205/772/2/114
- Wilber, M., Parks, G. K., Meziane, K., Lin, N., Lee, E., Mazelle, C., & Harris, A. (2008). Foreshock density holes in the context of known upstream plasma structures. *Annals of Geophysics*, 26, 3741–3755. https://doi.org/10.5194/angeo-26-3741-2008
- Wilson, L. B., III (2016). Low frequency waves at and upstream of collisionless shocks. In A. Keiling, D.-H. Lee, & V. Nakariakov (Eds.), Low frequency waves at and upstream of collisionless shocks. In low-frequency waves in space plasmas (pp. 269–291). https://doi.org/10.1002/9781119055006.ch16
- Zhang, H., Sibeck, D. G., Zong, Q.-G., Gary, S. P., McFadden, J. P., Larson, D., et al. (2010). Time History of Events and Macroscale Interactions during Substorms observations of a series of hot flow anomaly events. *Journal of Geophysical Research*, 115, A12235. https://doi.org/10.1029/2009JA015180
- Zhang, H., Sibeck, D. G., Zong, Q.-G., Omidi, N., Turner, D., & Clausen, L. B. N. (2013). Spontaneous hot flow anomalies at quasi-parallel shocks: 1. Observations. *Journal of Geophysical Research: Space Physics*, 118, 3357–3363. https://doi.org/10.1002/jgra.50376
- Zhang, H., Zong, Q.-G., Connor, H., Delamere, P., Facsk, G., Han, D., et al. (2022). Dayside transient phenomena and their impact on the magnetosphere and ionosphere. *Space Science Reviews*. https://doi.org/10.1007/s11214-021-00865-0
- Zhao, L. L., Zhang, H., & Zong, Q.-G. (2017). A statistical study on hot flow anomaly current sheets. *Journal of Geophysical Research: Space Physics*, 122, 235–248. https://doi.org/10.1002/2016JA023319

LU ET AL. 11 of 11